Long-distance genuine multipartite entanglement between magnetic defects in spin chains

Mirko Consiglio,[1] Jovan Odavić,[2,3] Riccarda Bonsignori,[4] Gianpaolo Torre,[5] Marcin Wieśniak,[6,7] Fabio Franchini,[5] Salvatore M. Giampaolo,[5,*] and Tony J. G. Apollaro[1]

[1]*Department of Physics, University of Malta, Msida MSD 2080, Malta*

[2]*INFN, Sezione di Napoli, Naples, Italy*

[3]*Dipartimento di Fisica "Ettore Pancini," Università degli Studi di Napoli Federico II, Via Cintia 80126, Naples, Italy*

[4]*Institute of Theoretical and Computational Physics, Graz University of Technology, Petersgasse 16, 8010 Graz, Austria*

[5]*Institut Ruđer Bošković, Bijenička cesta 54, 10000 Zagreb, Croatia*

[6]*Institute of Theoretical Physics and Astrophysics, Faculty of Mathematics, Physics, and Informatics, University of Gdańsk, 80-308 Gdańsk, Poland*

[7]*International Centre for Theory of Quantum Technologies, University of Gdańsk, 80-308 Gdańsk, Poland*

(Received 23 January 2025; accepted 11 March 2025; published 28 March 2025)

We investigate the emergence and properties of long-distance genuine multipartite entanglement, induced via three localized magnetic defects, in a one-dimensional transverse-field XX spin-1/2 chain. Using both analytical and numerical techniques, we determine the conditions for the existence of bound states localized at the defects. We find that the reduced density matrix (RDM) of the defects exhibits long-distance genuine multipartite entanglement (GME) across the whole range of the Hamiltonian parameter space, including regions where the two-qubit concurrence is zero. We quantify the entanglement by using numerical lower bounds for the GME concurrence, as well as by analytically deriving the GME concurrence in regions where the RDM is of rank 2. Our work provides insights into generating multipartite entanglement in many-body quantum systems via local control techniques.

DOI: 10.1103/PhysRevA.111.032434

I. INTRODUCTION

Multipartite entanglement is a fundamental resource in a variety of quantum information protocols, including multiparty quantum key distribution [1], quantum teleportation and dense coding [2], quantum metrology [3], and quantum computation [4]. Such centrality in a field so relevant as quantum information has attracted numerous works aimed at its quantification under different conditions. While significant progress has been made in characterizing and quantifying multipartite entanglement in pure states, such as identifying inequivalent classes under stochastic local operations and classical communication (SLOCC) [5–7] and developing related measures [8], studying multipartite entanglement in mixed states remains challenging [9–14] and an open problem. A variety of different avenues for tackling mixed-state multipartite entanglement have been proposed, from semidefinite programming [15] to geometric approaches [16] and witnesses [17]. By exploiting such quantities, it is now possible to investigate the multipartite entanglement in ground states of many-body systems, and many results for spin-1/2 models have already been published over the years [18–21]. Thanks to these advancements, the general behaviors of multipartite entanglement are well known. Among them, one of the most relevant is the fact that multipartite entanglement, similar to the bipartite one, is limited in range when evaluated for ground states of local Hamiltonians with short-range interactions.

Although the spatial range at which two spins have nonzero concurrence can be extended by breaking the translational invariance of the model, e.g., by modifying the edge [22–25] or the on-site couplings [26–28], the applicability of a similar approach to extend the range of multipartite entanglement has not been thoroughly investigated thus far. General results for the achievability of multipartite entanglement at an infinite distance were presented by Parez and Witczak-Krempa [29]. In this paper, we seek to address this gap by addressing the problem of generating long-distance multipartite entanglement among three magnetic defects embedded in the XX spin-1/2 Hamiltonian. In our approach, the defects are represented by a magnetic field in the transverse direction on three sites different from the rest of the system. We investigate the various classes of multipartite entanglement as a function of both the bulk's and defects' magnetic field intensities and the defects' distance, using a combination of analytical tools, lower-bound techniques, and entanglement witnesses. Interestingly, we show how the presence of the magnetic defects defines regions in the Hamiltonian's parameter space where discrete energy eigenstates, associated with localized states, appear in its spectrum. These eigenstates can sustain long-distance genuine multipartite entanglement (GME), which can be quantified with GME concurrence [30], regardless of the relative distance between the defects.

This paper is organized as follows: In Sec. II we introduce the XX spin-1/2 model with magnetic defects and define the

*Contact author: sgiampa@irb.hr

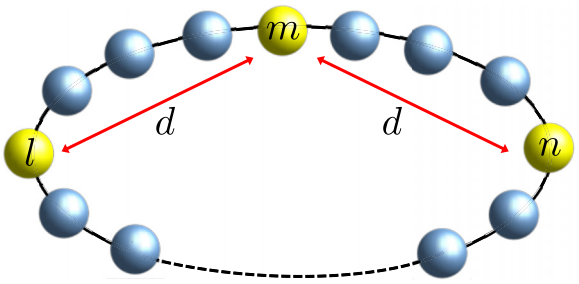

FIG. 1. Spin-1/2 chain with periodic boundary conditions of even size N, described by the Hamiltonian in Eq. (1), where on sites l, m, and n (the defects) an additional magnetic field ε is applied. Defects l and n are equidistant from the defect located at site m.

regions exhibiting discrete eigenenergies; in Sec. III we derive the reduced density matrix (RDM) of the defects' subsystem and define the figures of merit for tripartite genuine multipartite entanglement that are used in Sec. IV to present our main result about long-distance GME concurrence. In Sec. V we conclude the paper and discuss prospects for further research.

II. THE MODEL

We consider the one-dimensional XX spin-1/2 chain in a transverse magnetic field h, which is uniform everywhere except for three spins, located at sites $k + jd$ ($j = -1, 0, 1$), hereafter dubbed "defects." The Hamiltonian describing the system's dynamics consists of two distinct components:

$$\hat{H} = \hat{H}_{\mathrm{XX}} + \hat{H}_{\mathrm{def}}. \tag{1}$$

The first is a homogeneous XX Hamiltonian,

$$\hat{H}_{\mathrm{XX}} = \frac{J}{2}\sum_{i=1}^{N}\left(\hat{\sigma}_i^x\hat{\sigma}_{i+1}^x + \hat{\sigma}_i^y\hat{\sigma}_{i+1}^y\right) - \frac{h}{2}\sum_{i=1}^{N}\hat{\sigma}_i^z, \tag{2}$$

where J is the coupling constant, which from here on we assume to be equal to 1; h is the transverse field; $\hat{\sigma}_i^\alpha$, with $\alpha = x, y, z$, are the Pauli operators acting on the ith spin; and periodic boundary conditions are imposed ($\hat{\sigma}_i^\alpha = \hat{\sigma}_{i+N}^\alpha$). In the thermodynamic limit, the model in Eq. (2) admits a first-order quantum phase transition that separates a gapped paramagnetic phase characterizing the region $|h| > 2$ from a gapless critical phase for $|h| \leqslant 2$. The second term is the translational symmetry-breaking term given by

$$\hat{H}_{\mathrm{def}} = \frac{\varepsilon}{2}\sum_{j=-1}^{1}\hat{\sigma}_{k+jd}^z, \tag{3}$$

as depicted in Fig. 1. In Eq. (3), ε stands for the strength of the defects, and d is the relative distance between them that we assume is much smaller than the size of the system, i.e., $d \ll N$. The Hamiltonian in Eq. (1) holds several symmetry properties. However, for our purposes, it is worth noting that $\hat{H}$ possesses U(1) symmetry, implying that the total magnetization along the z axis is conserved, i.e., $[\hat{H}, \sum_i \hat{\sigma}_i^z] = 0$.

Regardless of the presence of defects, the model in Eq. (1) can be mapped into a quadratic Hamiltonian of spinless fermions, with annihilation and creation operators given by $\hat{c}_i$ and $\hat{c}_i^\dagger$, respectively, via the Jordan-Wigner transformation [31],

$$H = J\sum_{i=1}^{N-1}(c_i^\dagger c_{i+1} + c_{i+1}^\dagger c_i) + \hat{P}_z(c_1^\dagger c_N + c_N^\dagger c_1) - h\sum_{i=1}^{N}c_i^\dagger c_i + \varepsilon\sum_{j=-1}^{1}c_{k+jd}^\dagger c_{k+jd}. \tag{4}$$

Here, $\hat{P}_z$ stands for the parity operator along z with eigenvalues ± 1. Hence, depending on the total magnetization of the state, it induces antiperiodic or periodic boundary conditions [32,33]. In the following, we will consider only the positive-parity subspace because the RDM of the three defects whose entanglement properties we investigate are equivalent to $N \gg 1$.

Because of its quadratic nature, the Hamiltonian in Eq. (4) is readily diagonalized as

$$\hat{H} = \sum_{k=1}^{N}\omega_k\hat{c}_k^\dagger\hat{c}_k, \tag{5}$$

where ω_k and $\hat{c}_k^\dagger = \sum_n \phi_{kn}\hat{c}_n$ are, respectively, the single-particle eigenenergies and eigenstates of the fermionic problem. In the limit $\varepsilon \to 0$ we recover $\omega_k = h - 2\cos(2\pi k/N)$, and in the thermodynamic limit, the single-particle spectrum makes up a continuous band with $\omega_k \in [h-2, h+2]$, with the eigenstates encoding plane waves [34]. In contrast, taking into account a strictly positive value of ε, up to three discrete energy levels emerge from below the band. Using a Green's function approach [35], it is possible to analytically determine the boundaries $\varepsilon(d)$ between the regions with one, two, and three discrete eigenstates of the Hamiltonian. Those regions are

$$0 < \varepsilon < \frac{1}{d}, \tag{6a}$$

$$\frac{1}{d} < \varepsilon < \frac{3}{d}, \tag{6b}$$

$$\frac{3}{d} < \varepsilon \tag{6c}$$

for one, two, and three discrete energy levels, respectively. The details of the derivation of these results can be found in the Appendix. In Fig. 2 we show the energy spectrum of the fermionic Hamiltonian in Eq. (4), with $h = 2$ and $J = 1$, as a function of the product εd, where it is possible to have the emergence of discrete single-particle energies. Changing h, the single-particle energy spectrum is shifted vertically. Different from the ones in the band, the eigenstates corresponding to the discrete eigenenergies are exponentially localized on the defects [36]. In contrast, the continuous energy band gets distorted, and its eigenstates acquire a contribution describing backscattering at the impurity sites [35,37]. From Eq. (6) it is possible to identify three different regions in the ε-d plane, each one of them characterized by a different number of localized states. These regions are depicted in Fig. 3.

III. MULTIPARTITE ENTANGLEMENT

As already mentioned, the main goal of this work is to study the multipartite entanglement in the ground state of

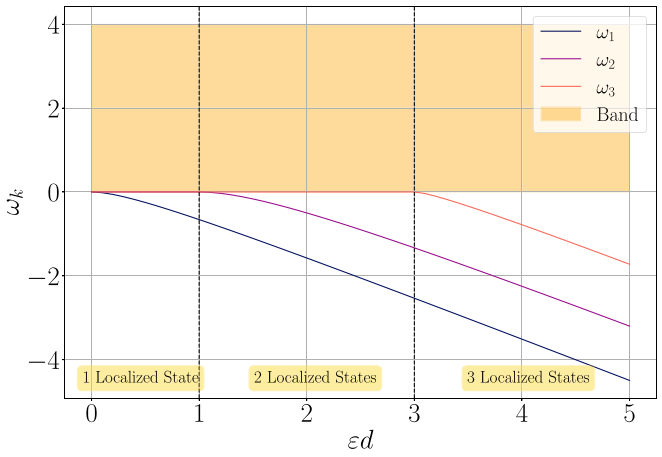

FIG. 2. Single-particle energy spectrum for $h = 2$ illustrating the emergence of discrete energy levels below the continuous band as a function of ε for $d = 1$.

the model in Eq. (1) between the spins on which magnetic defects are present. Toward this end, we first need to evaluate the RDM that is obtained by tracing out all the degrees of freedom associated with the spins on which no defects are present. The form of this matrix will take into account all the symmetries of the state from which it is obtained. In our case, it is well-known that the ground state of the XX model with periodic boundary conditions, as in Eq. (2), has a vanishing momentum that implies that the RDM is real [33]. This result remains unaffected by the presence of defects. Moreover, since the distance between the first and second defects and that between the second and the third are equal, there is a reflection symmetry with respect to the central defect. Furthermore, the Hamiltonian in Eq. (1) preserves the global magnetization, and therefore, all its eigenstates, including the ground state, have a well-determined value of total magnetization. Taking into account all these properties, the RDM in the

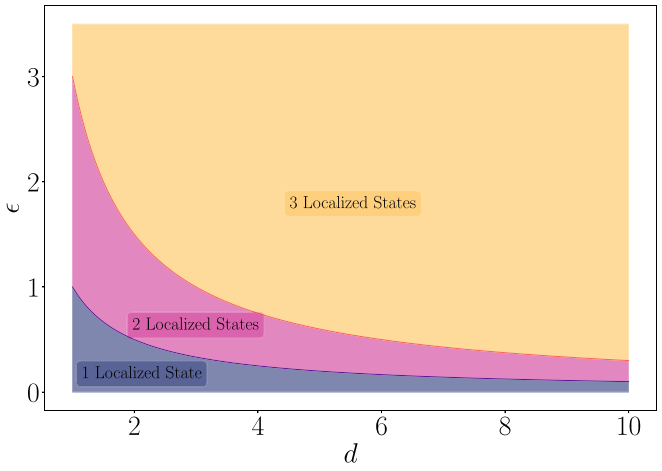

FIG. 3. Illustration showcasing the regions where one, two, and three localized states appear in the $\varepsilon - d$ plane. The curve between the regions of one and two localized states is given by $\varepsilon = 1/d$, and the curve between the regions of two and three localized states is given by $\varepsilon = 3/d$.

computational basis becomes

$$\hat{\rho} = \begin{pmatrix} \rho_{00} & 0 & 0 & 0 & 0 & 0 & 0 & 0 \\ 0 & \rho_{11} & \rho_{12} & 0 & \rho_{14} & 0 & 0 & 0 \\ 0 & \rho_{12} & \rho_{22} & 0 & \rho_{12} & 0 & 0 & 0 \\ 0 & 0 & 0 & \rho_{33} & 0 & \rho_{35} & \rho_{36} & 0 \\ 0 & \rho_{14} & \rho_{12} & 0 & \rho_{11} & 0 & 0 & 0 \\ 0 & 0 & 0 & \rho_{35} & 0 & \rho_{55} & \rho_{35} & 0 \\ 0 & 0 & 0 & \rho_{36} & 0 & \rho_{35} & \rho_{33} & 0 \\ 0 & 0 & 0 & 0 & 0 & 0 & 0 & \rho_{77} \end{pmatrix}. \tag{7}$$

This matrix is, in general, a rank-8 density matrix that can be decomposed as follows:

$$\hat{\rho} = p_0 |000\rangle\langle 000| + \sum_{i=1}^{3} p_i |gW_i\rangle\langle gW_i| + \sum_{i=1}^{3} \bar{p}_i |g\bar{W}_i\rangle\langle g\bar{W}_i| + p_7 |111\rangle\langle 111|, \tag{8}$$

where $|gW_i\rangle$ and $|g\bar{W}_i\rangle$ are, respectively, the generalized W and the generalized spin-flipped W states,

$$|gW_i\rangle = a_1^{(i)} |001\rangle + a_2^{(i)} |010\rangle + a_3^{(i)} |100\rangle , \tag{9}$$

$$|g\bar{W}_i\rangle = b_1^{(i)} |011\rangle + b_2^{(i)} |101\rangle + b_3^{(i)} |110\rangle . \tag{10}$$

This decomposition is particularly useful since it allows us to prove that the three-tangle [38] of ρ vanishes, i.e., $\tau_3(\rho) = 0$. Such a result follows straightforwardly from the convex-roof extension of τ_3 to mixed states [39] and from the well-known results that for a generalized W state, τ_3 is identically zero. This restricts the possibility of genuine multipartite entanglement to W type [40], which has $\tau_3 = 0$ but finite GME concurrence $\mathcal{C}_{\mathrm{GME}}$ [30]. The GME concurrence for pure states is defined as

$$\mathcal{C}_{\mathrm{GME}}(|\psi\rangle) = \min_i \sqrt{2\left(1 - \mathrm{Tr}\left\{\rho_i^2\right\}\right)}, \tag{11}$$

where ρ_i is the RDM of the ith bipartition. For mixed states, similar to the three-tangle, the GME concurrence can be calculated by exploiting the convex-roof extension,

$$\mathcal{C}_{\mathrm{GME}}(\rho) = \inf \sum_i p_i \mathcal{C}_{\mathrm{GME}}(|\Psi_i\rangle), \tag{12}$$

such that $\rho = \sum_i p_i |\Psi_i\rangle\langle\Psi_i|$ and the minimization procedure is carried out over all possible pure-state decompositions of ρ.

The computation of the GME concurrence for the case of more than one localized state (that is, when the rank of the density matrix is equal to or larger than 2) is a highly nontrivial problem, which makes the analytical solution challenging to obtain. Consequently, we resort to numerical techniques to determine a lower bound for the GME concurrence exploiting two different methods, one presented by Ma *et al.* [30] and one presented by Hong *et al.* [41]. Both algorithms were embedded within a Monte Carlo algorithm using 100 runs with random initial states, with the global minimum taken to be the one with the highest GME concurrence. The Broyden-Fletcher-Goldfarb-Shanno (BFGS) [42] optimizer was employed as the local optimizer, taken from the SCIPY library [43].

To complement the previous method, we also consider a separability criterion for the density matrix resorting to the algorithm presented by Hofmann *et al.* [44], which iteratively attempts to decompose a given density matrix ρ into a convex sum of biseparable components. At iteration $k+1$, the density matrix is expressed as the convex sum of k terms $|\psi_k\rangle\langle\psi_k|$, where $|\psi_k\rangle$ is a biseparable state, and an additional semidefinite matrix ρ_{k+1}. If, for a certain k, the condition

$$\mathcal{W} = \mathrm{Tr}\left(\rho_{k+1}^2\right) - \tfrac{1}{7} < 0 \tag{13}$$

is satisfied, the density matrix is separable with respect to some bipartition (see Gurvits and Barnum [45] for further details). The data are obtained by considering 1500 iterations with 1000 randomly generated biseparable states for each iteration.

Together with the multipartite entanglement, to have a complete characterization of ρ, we also have to evaluate the bipartite entanglement between each pair of spins. Such entanglement can easily be quantified by the concurrence [46]. Due to the symmetry in the model, the concurrence between the first and the second must be equal to the one from the second and the third, i.e., $\mathcal{C}_{12} = \mathcal{C}_{23}$. Since the partial trace of ρ with respect to any qubit is an X state (that is, the RDM is zero excepts along the two diagonals), we can determine the concurrence via the simplified expression provided by Amico *et al.* [47]. Accordingly, the concurrence between the first and second defects (and, similarly, between the second and third defects) is

$$\mathcal{C}_{12} = 2\max\{0, |\rho_{12}+\rho_{35}| - \sqrt{(\rho_{00}+\rho_{44})(\rho_{33}+\rho_{77})}\}, \tag{14}$$

while concurrence between the first and third defects is

$$\mathcal{C}_{13} = 2\max\{0, |\rho_{14}+\rho_{36}| - \sqrt{(\rho_{00}+\rho_{22})(\rho_{55}+\rho_{77})}\}. \tag{15}$$

IV. LONG-DISTANCE GME CONCURRENCE

As discussed in Sec. II, the XX model in Eq. (2) exhibits two distinct thermodynamic phases, a gapless one for $|h| \leqslant 2$ and a gapped one for $|h| > 2$. Therefore, it is natural to study the emergence of multipartite entanglement following the presence of defects in the two regions separately.

A. The paramagnetic phase

For $h \geqslant 2$, discrete eigenstates emerge from below the continuous band for any $\varepsilon > 0$ (see Fig. 2). For $0 < \varepsilon < 1/d$, only one discrete energy level is present. As a consequence, the reduced density matrix can be written as

$$\rho = p|gW\rangle\langle gW| + (1-p)|000\rangle\langle 000|, \tag{16}$$

which is of rank 2. This case is of particular interest since we can analytically determine the GME concurrence following the path depicted in Refs. [48,49]. We start by analyzing the GME concurrence of the family of pure states,

$$|p,\varphi\rangle = \sqrt{p}\,|gW\rangle + e^{i\varphi}\sqrt{1-p}\,|000\rangle\,, \tag{17}$$

where $0 \leqslant p \leqslant 1$ and $0 \leqslant \varphi \leqslant 2\pi$ can be considered free parameters. Using Eq. (11) and recalling the expression of the generalized W state in Eq. (9), the GME concurrence of these states is

$$\mathcal{C}_{\mathrm{GME}}(p,\varphi) = 2p\min\{|a_1|\sqrt{1-|a_1|^2}, |a_2|\sqrt{1-|a_2|^2}, |a_3|\sqrt{1-|a_3|^2}\}. \tag{18}$$

As a result, the zero polytope [50] of the states in Eq. (18) is a trivial one, where $p = 0$, assuming $|a_1|, |a_2|, |a_3| \neq 0, 1$. The next step is to construct the convex characteristic curve [50]. Since $0 \leqslant |a_1|, |a_2|, |a_3| \leqslant 1$, $\mathcal{C}_{\mathrm{GME}}(p,\varphi)$ monotonically increases with p and is invariant with respect to φ. Moreover, $\mathcal{C}_{\mathrm{GME}}(p,\varphi)$ also linearly increases with p, which implies that it is already convex. As a result, the GME concurrence is equal to the weight of the generalized W state, similar to how the concurrence between a Bell state and an unentangled state is equal to the weight of the Bell state [51]. Therefore,

$$\mathcal{C}_{\mathrm{GME}}(\rho) = 2p\min\{|a_1|\sqrt{1-|a_1|^2}, |a_2|\sqrt{1-|a_2|^2}, |a_3|\sqrt{1-|a_3|^2}\}. \tag{19}$$

In our case, due to the symmetry properties of our system, a_3 is equal to a_1, and $a_2 = \sqrt{1-2a_1^2}$, with $a_1 \in [0, 1/\sqrt{2}]$. Thus, the GME concurrence reduces to

$$\begin{aligned}\mathcal{C}_{\mathrm{GME}}(\rho) &= 2a_1 p\min\left\{\sqrt{1-a_1^2}, \sqrt{2-4a_1^2}\right\} \\ &= 2\min\{\sqrt{2}|\rho_{12}|, \sqrt{|\rho_{14}|(1-\rho_{00}-|\rho_{14}|)}\}.\end{aligned} \tag{20}$$

It has to be noted that, due to the range of values of a_1, ρ always has a nonzero GME concurrence independent of the distance d, although it becomes vanishingly small as the distance increases. This dependence on the distance can be appreciated in Fig. 4, where we show the GME concurrence $\mathcal{C}_{\mathrm{GME}}$ as a function of the rescaled defects' intensity εd in the region with a single localized energy eigenstate.

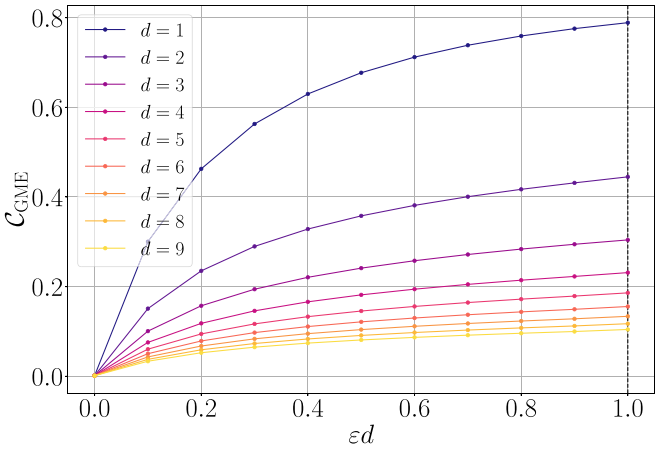

FIG. 4. Analytically determined GME concurrence as a function of εd in the presence of one localized state.

For $\varepsilon > 1/d$, more localized states appear in the ground state of the system, and the rank of the RDM increases. This makes finding the convex-roof extension via analytical methods as done above for rank-2 density matrices highly nontrivial. Therefore, in the following, we resort to the numerical methods described in the previous section to determine the lower bound of the GME concurrence and corroborate our

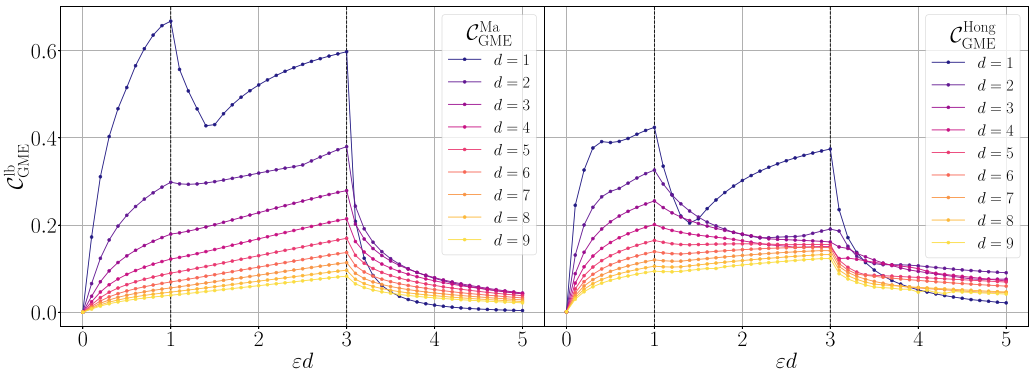

FIG. 5. Lower bound on the GME concurrence as a function of εd for defects at a distance of up to 9 and $h = 2$. Left: Bound given by Ma *et al.* [30]. Right: Bound given by Hong *et al.* [41]. The vertical lines at $\varepsilon d = 1$ and $\varepsilon d = 3$ determine the boundaries between one and two localized eigenstates and between two and three localized eigenstates, respectively.

results by evaluating the separability criterion (13) of genuine multipartite entanglement.

Figure 5 shows the lower bound of the GME concurrence for $h = 2$ as a function of ϵd. For completeness, we also compute this bound for the previous case of only one localized eigenstate ($0 < \varepsilon d < 1$). We notice that, although the lower bounds of the GME concurrence decrease as the defects' separation d increases, they remain finite, indicating that long-distance GME concurrence is attainable for every value of ε and d. Hence, the numerically derived bounds for $\varepsilon d > 1$ confirm the presence of GME concurrence when multiple localized states contribute to the ground state. To strengthen these findings, we also consider the separability criterion (13), which complements the GME results (Fig. 6). We always found $\mathcal{W} \geqslant 0$; that is, the state is not separable for any bipartition. Finally, we also used the separability criterion based on the Hilbert-Schmidt distance developed in Ref. [52], and strong numerical evidence suggests a nonzero distance to the closest biseparable state. These results emphasize the ability of the defects to sustain long-distance multipartite entanglement that would otherwise be absent in uniform systems.

In Fig. 7 we show the concurrence between the defects as evaluated with Eqs. (14) and (15). While the concurrence between adjacent defects $\mathcal{C}_{12}$ and $\mathcal{C}_{23}$ is nonzero for smaller εd, it vanishes beyond $\varepsilon d > 3$ and $d > 1$. Similarly, the concurrence between the outer defects $\mathcal{C}_{13}$ is negligible for most of the parameter space. As a consequence, density matrices of the form of Eq. (7) can sustain states with nonzero GME concurrence and vanishing two-qubit concurrence, similar to X-type states [53].

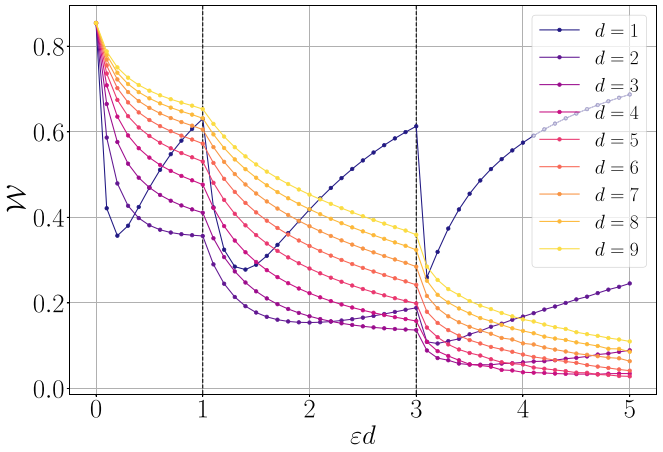

FIG. 6. Witness $\mathcal{W}$ in Eq. (13) as a function of ϵd for $h = 2$ and for different distances between the defects.

B. The critical phase

For any $|h| \leqslant 2$, regardless of the value of $\varepsilon \geqslant 0$, the RDM is always of rank 8, preventing an analytical determination of the GME concurrence. However, like in Sec. IV A above, we report the two lower bounds presented by Ma *et al.* [30] and Hong *et al.* [41], the respective concurrences $\mathcal{C}_{12}$ and $\mathcal{C}_{23}$, and the separability criterion in Eq. (13). Figure 8 shows the lower bounds for the GME concurrence, and Fig. 9 shows the separability witness for $h = 1$. Like in the case of $h = 2$, nonzero long-distance entanglement is present for any value of εd also in the absence of any pairwise concurrence between the qubits, which vanishes for $d > 1$ and $\varepsilon > 0$.

V. CONCLUSION

In this work, we studied the interplay between magnetic defects and multipartite entanglement in an XX spin-1/2 chain subjected to a transverse field. Using analytical techniques complemented by numerical methods, we characterized the emergence of localized bound states at the defect sites.

Our findings demonstrate the existence of regions in parameter space, defined by the defect intensity and separation, where GME arises. For a single localized state, the GME concurrence was derived analytically. When multiple localized states were present, numerical approaches were employed to establish lower bounds on GME concurrence and validate multipartite entanglement through separability witnesses.

Interestingly, while pairwise entanglement between defects vanishes in certain regions, the GME concurrence persists, underscoring the robustness of multipartite entanglement at larger defect separations. This allows for the generation of long-distance multipartite entanglement in a many-body system with nearest-neighbor interaction by the application of

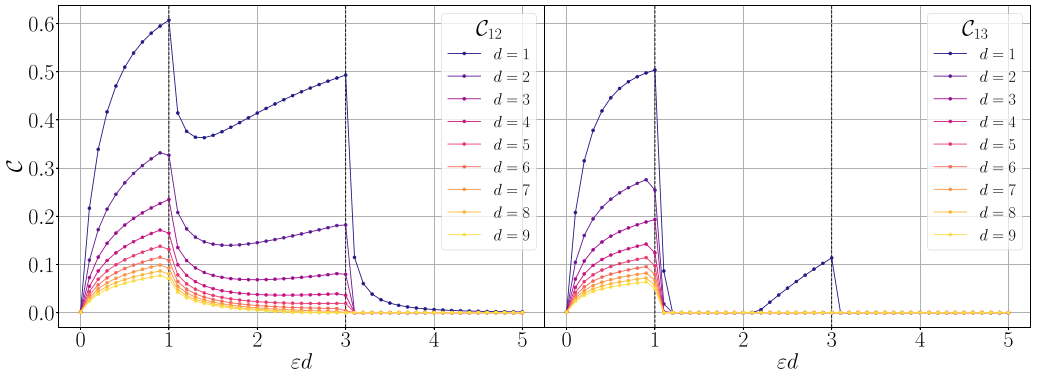

FIG. 7. Two-qubit concurrence as a function of εd for defects at a distance of up to 9 and $h = 2$. Left: Concurrence between defects 1 and 2 (equivalent to the concurrence between defects 2 and 3). Right: Concurrence between defects 1 and 3. The vertical lines at $\varepsilon d = 1$ and $\varepsilon d = 3$ determine the boundaries between one and two localized eigenstates and between two and three localized eigenstates, respectively.

local magnetic defects at desired locations. This approach to the generation of multipartite entanglement appears simultaneously easier and more flexible than the one based on models with cluster interactions [54,55], hence revealing a path to possible technological applications in quantum communication and quantum technologies. In addition to such applications, our analytic results and numerical lower bounds shed light on the properties of multipartite entanglement in density matrices without coherence between different magnetization sectors, where only W-type entanglement can be present.

Although we restricted our analysis to three defects, the proposed method for long-distance multipartite entanglement generation via local magnetic fields can be straightforwardly extended to a higher number of defects to investigate higher SLOCC entanglement classes [6] or to the XY model, which sustains Greenberger-Horne-Zeilinger-type entanglement [20].

ACKNOWLEDGMENTS

M.C. acknowledges funding from the Tertiary Education Scholarships Scheme MFED 758/2021/34. M.C. and T.J.G.A. acknowledge Xjenza Malta for their support via the project GROUNDS IPAS-2023-059 and thank P. Erker for useful discussions on the GME concurrence lower bounds. J.O. acknowledges the support from PNRR MUR Project No. PE0000023-NQSTI and thanks V. Eisler for useful discussions. R.B. acknowledges support from Croatian Science Foundation (HrZZ) Project No. IP-2019-4-3321 and Austrian Science Fund (FWF) Grant DOI: 10.55776P35434. M.W. acknowledges the support from NCN (Poland) Grant No. 2017/26/E/ST2/01008.

DATA AVAILABILITY

The data that support the findings of this article are openly available [56]. Data that are not openly available are available upon reasonable request from the authors.

APPENDIX: GREEN'S FUNCTIONS METHOD

We consider the one-dimensional (1D) tight-binding Hamiltonian in the presence of three impurities, corresponding to the one in Eq. (4), decomposed as

$$H = H_0 + H_1, \tag{A1}$$

where H_0 is the tight-binding Hamiltonian without impurities, characterized by nearest-neighbor interactions

$$H_0 = \sum_i h|i\rangle\langle i| + J\sum_i (|i\rangle\langle i+1| + \text{H.c.}), \tag{A2}$$

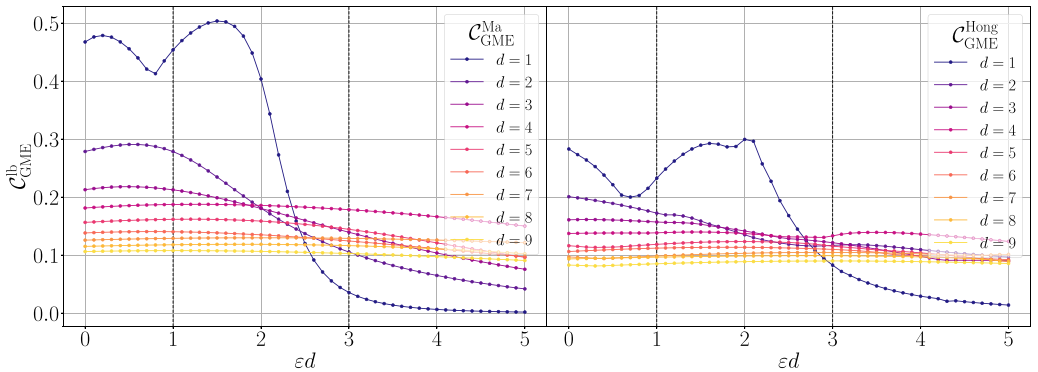

FIG. 8. Lower bound on the GME concurrence as a function of εd for defects at a distance of up to 9 and $h = 1$. Left: Bound given by Ma *et al.* [30]. Right: Bound given by Hong *et al.* [41]. The vertical lines at $\varepsilon d = 1$ and $\varepsilon d = 3$ determine the boundaries between one and two localized eigenstates and between two and three localized eigenstates, respectively.

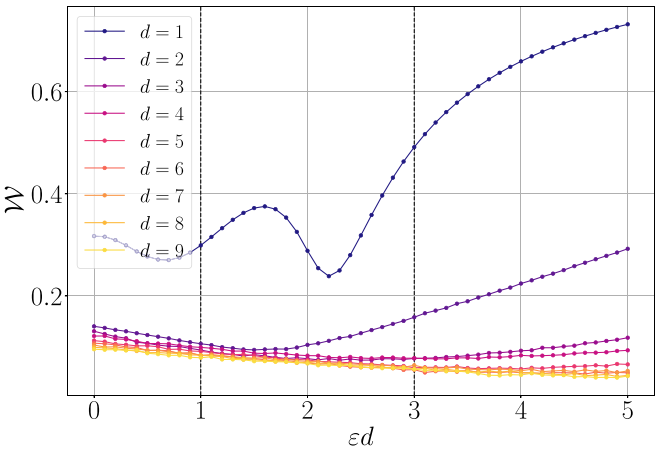

FIG. 9. Witness $\mathcal{W}$ in Eq. (13) as a function of ϵd for $h = 1$ and for different distances between the defects.

and $H_1 = H_l + H_m + H_n$ denotes the perturbation, which is assumed to be diagonal,

$$H_1 = \varepsilon_l |l\rangle\langle l| + \varepsilon_m |m\rangle\langle m| + \varepsilon_n |n\rangle\langle n|. \tag{A3}$$

We introduce the unperturbed Green's operator G_0 corresponding to H_0,

$$G_0(z) = \frac{1}{z - H_0} = \sum_k \frac{|k\rangle\langle k|}{z - E_k}. \tag{A4}$$

In the limit $N \to \infty$, the set of states $|k\rangle$ forms a continuous band with energies $E_k \in I_b = [2h - J, 2h + J]$. The matrix elements of G_0 between two localized states are given by

$$G_0(r, s; z) = \frac{(-x + \sqrt{x^2 - 1})^{|r-s|}}{J\sqrt{x^2 - 1}}, \quad z \notin I_b, \tag{A5}$$

and

$$G_0(r, s; z) = \frac{(-x \pm \imath\sqrt{1 - x^2})^{|r-s|}}{\pm\imath J\sqrt{x^2 - 1}}, \quad z \in I_b, \tag{A6}$$

where $x = \frac{z-2h}{J}$. The full Green's operator G, corresponding to the full Hamiltonian H, can be obtained as

$$G = G_0 + G_0 T G_0, \tag{A7}$$

where the T matrix is determined from the knowledge of G_0 and H_1 as

$$T = H_1 + H_1 G_0 H_1 + H_1 G_0 H_1 G_0 H_1 + \cdots. \tag{A8}$$

The T matrix can be obtained following the approach in [35]. Introducing the unit operator into Eq. (A8), we get

$$T = H_1 + H_1 \sum_i |i\rangle\langle i| G_0 \sum_{i'} |i'\rangle\langle i'| H_1 + \cdots. \tag{A9}$$

Since the defects are diagonal, we need to retain in the summation only the terms $(|l\rangle\langle l| + |m\rangle\langle m| + |n\rangle\langle n|)$, which can be written as a scalar product $|\alpha\rangle\langle\alpha|$, with

$$|\alpha\rangle \equiv [|l\rangle, |m\rangle, |n\rangle], \quad \langle\alpha| \equiv \begin{bmatrix} \langle l| \\ \langle m| \\ \langle n| \end{bmatrix}. \tag{A10}$$

With this notation, we have

$$\langle\alpha| T |\alpha\rangle = \langle\alpha| H_1 |\alpha\rangle (\mathbb{I}_3 - \langle\alpha| G_0 |\alpha\rangle \langle\alpha| H_1 |\alpha\rangle)^{-1}, \tag{A11}$$

where

$$\langle\alpha| H_1 |\alpha\rangle = \begin{pmatrix} \varepsilon_l & 0 & 0 \\ 0 & \varepsilon_m & 0 \\ 0 & 0 & \varepsilon_n \end{pmatrix}, \tag{A12}$$

$$\langle\alpha| G_0 |\alpha\rangle = \begin{pmatrix} G_0(l,l) & G_0(l,m) & G_0(l,n) \\ G_0(m,l) & G_0(m,m) & G_0(m,n) \\ G_0(n,l) & G_0(n,m) & G_0(n,n) \end{pmatrix}. \tag{A13}$$

The first step is to invert the matrix

$$\mathbb{I}_3 - \langle\alpha| G_0 |\alpha\rangle \langle\alpha| H_1 |\alpha\rangle = \begin{pmatrix} [1 - \varepsilon_l G_0(l,l)] & -\varepsilon_m G_0(l,m) & -\varepsilon_n G_0(l,n) \\ -\varepsilon_l G_0(m,l) & [1 - \varepsilon_m G_0(m,m)] & -\varepsilon_n G_0(m,n) \\ -\varepsilon_l G_0(n,l) & -\varepsilon_m G_0(n,m) & [1 - \varepsilon_n G_0(n,n)] \end{pmatrix}. \tag{A14}$$

The determinant gives

$$\det[\mathbb{I}_3 - \langle\alpha| G_0 |\alpha\rangle \langle\alpha| H_1 |\alpha\rangle] = f_{lmn}^{-1}[1 - \varepsilon_l G_0(l,l)][1 - \varepsilon_m G_0(m,m)][1 - \varepsilon_n G_0(n,n)], \tag{A15}$$

where we define f_{lmn} as

$$f_{lmn} = \{1 - t_l t_m G_0(l,m) G_0(m,l) - t_m t_n G_0(m,n) G_0(n,m) - t_n t_l G_0(n,l) G_0(l,n) - t_l t_m t_n [G_0(l,m) G_0(m,n) G_0(n,l) + G_0(m,l) G_0(l,n) G_0(n,m)]\}^{-1} \tag{A16}$$

and

$$t_j = \frac{\varepsilon_j}{1 - \varepsilon_j G_0(j,j)}, \quad j = l, m, n. \tag{A17}$$

The poles of the Green's functions for the three-defect problem can be determined from the zeros of Eq. (A16). In the case with $\varepsilon_l = \varepsilon_m = \varepsilon_n$ and $|l - m| = |n - m| = d$, that is, the intensities of the magnetic field on the three defects are the same and the defects are symmetrically placed around the central defect, as in Fig. 2 in the main text, we find, using the *Mathematica* software package and confirmed by numerical simulations, that for $0 < \varepsilon < 1/d$ only one solution is found, for $1 < \varepsilon < 3/d$ two solutions are found, and for $3/d < \varepsilon$ three solutions are found, as reported in Eq. (6) in the main text.

The emergence of three localized states can also be obtained by solving the 1D Schrodinger equation with three δ potentials:

$$-\frac{d^2\psi(x)}{dx^2} + V(x)\psi(x) = E\psi(x), \tag{A18}$$

where the potential is

$$V(x) = -\varepsilon[\delta(x + d) + \delta(x) + \delta(x - d)]. \tag{A19}$$

Straightforward calculations give the solutions for bound states of this problem as

$$0 < d < \frac{\hbar^2}{2m\varepsilon} \tag{A20a}$$

for one even solution,

$$\frac{\hbar^2}{2m\varepsilon} < d < \frac{3\hbar^2}{2m\varepsilon} \tag{A20b}$$

for one odd solution and one even solution, and

$$\frac{3\hbar^2}{2m\varepsilon} < d \tag{A20c}$$

for one odd and two even solutions,
and by setting $\hbar^2/2m = 1$, we obtain Eq. (6).

[1] M. Epping, H. Kampermann, C. macchiavello, and D. Bruß, Multi-partite entanglement can speed up quantum key distribution in networks, New J. Phys. **19**, 093012 (2017).

[2] Y. Yeo and W. K. Chua, Teleportation and dense coding with genuine multipartite entanglement, Phys. Rev. Lett. **96**, 060502 (2006).

[3] G. Tóth, Multipartite entanglement and high-precision metrology, Phys. Rev. A **85**, 022322 (2012).

[4] R. Raussendorf and H. J. Briegel, A one-way quantum computer, Phys. Rev. Lett. **86**, 5188 (2001).

[5] W. Dür, G. Vidal, and J. I. Cirac, Three qubits can be entangled in two inequivalent ways, Phys. Rev. A **62**, 062314 (2000).

[6] F. Verstraete, J. Dehaene, B. De Moor, and H. Verschelde, Four qubits can be entangled in nine different ways, Phys. Rev. A **65**, 052112 (2002).

[7] P. Horodecki, L. Rudnicki, and K. Życzkowski, Multipartite entanglement, arXiv:2409.04566.

[8] M. Ma, Y. Li, and J. Shang, Multipartite entanglement measures: A review, Fundam. Res. (2024), doi:10.1016/j.fmre.2024.03.031.

[9] M. Huber, P. Erker, H. Schimpf, A. Gabriel, and B. Hiesmayr, Experimentally feasible set of criteria detecting genuine multipartite entanglement in n-qubit Dicke states and in higher-dimensional systems, Phys. Rev. A **83**, 040301(R) (2011).

[10] M. Walter, D. Gross, and J. Eisert, Multipartite entanglement, in *Quantum Information* (Wiley, Hoboken, NJ, 2016), Chap. 14, pp. 293–330.

[11] C. Eltschka and J. Siewert, Quantifying entanglement resources, J. Phys. A **47**, 424005 (2014).

[12] I. Bengtsson and K. Życzkowski, *Geometry of Quantum States* (Cambridge University Press, Cambridge, 2017).

[13] L. Lepori, A. Trombettoni, D. Giuliano, J. Kombe, J. Yago Malo, A. J. Daley, A. Smerzi, and M. Luisa Chiofalo, Can multipartite entanglement be characterized by two-point connected correlation functions? J. Phys. A **56**, 305302 (2023).

[14] M. Wieśniak, Multipartite entanglement versus multiparticle entanglement, arXiv:2407.13348.

[15] B. Jungnitsch, T. Moroder, and O. Gühne, Taming multiparticle entanglement, Phys. Rev. Lett. **106**, 190502 (2011).

[16] M. Cianciaruso, T. R. Bromley, and G. Adesso, Accessible quantification of multiparticle entanglement, npj Quantum Inf. **2**, 16030 (2016).

[17] J. Sperling and W. Vogel, Multipartite entanglement witnesses, Phys. Rev. Lett. **111**, 110503 (2013).

[18] O. Gühne, G. Tóth, and H. J. Briegel, Multipartite entanglement in spin chains, New J. Phys. **7**, 229 (2005).

[19] L. Amico, R. Fazio, A. Osterloh, and V. Vedral, Entanglement in many-body systems, Rev. Mod. Phys. **80**, 517 (2008).

[20] S. M. Giampaolo and B. C. Hiesmayr, Genuine multipartite entanglement in the XY model, Phys. Rev. A **88**, 052305 (2013).

[21] Z. Liu, Y. Tang, H. Dai, P. Liu, S. Chen, and X. Ma, Detecting entanglement in quantum many-body systems via permutation moments, Phys. Rev. Lett. **129**, 260501 (2022).

[22] L. Campos Venuti, C. Degli Esposti Boschi, and M. Roncaglia, Long-distance entanglement in spin systems, Phys. Rev. Lett. **96**, 247206 (2006).

[23] S. M. Giampaolo and F. Illuminati, Long-distance entanglement and quantum teleportation in coupled-cavity arrays, Phys. Rev. A **80**, 050301(R) (2009).

[24] L. Campos Venuti, S. M. Giampaolo, F. Illuminati, and P. Zanardi, Long-distance entanglement and quantum teleportation in XX spin chains, Phys. Rev. A **76**, 052328 (2007).

[25] S. M. Giampaolo and F. Illuminati, Long-distance entanglement in many-body atomic and optical systems, New J. Phys. **12**, 025019 (2010).

[26] T. J. G. Apollaro and F. Plastina, Entanglement localization by a single defect in a spin chain, Phys. Rev. A **74**, 062316 (2006).

[27] F. Plastina and T. J. G. Apollaro, Local control of entanglement in a spin chain, Phys. Rev. Lett. **99**, 177210 (2007).

[28] T. J. Apollaro, A. Cuccoli, A. Fubini, F. Plastina, and P. Verrucchi, Staggered magnetization and entanglement enhancement by magnetic impurities in a $S = 1/2$ spin chain, Phys. Rev. A **77**, 062314 (2008).

[29] G. Parez and W. Witczak-Krempa, The fate of entanglement, arXiv:2402.06677.

[30] Z.-H. Ma, Z.-H. Chen, J.-L. Chen, C. Spengler, A. Gabriel, and M. Huber, Measure of genuine multipartite entanglement with computable lower bounds, Phys. Rev. A **83**, 062325 (2011).

[31] E. Lieb, T. Schultz, and D. Mattis, Two soluble models of an antiferromagnetic chain, Ann. Phys. (NY) **16**, 407 (1961).

[32] B. Damski and M. M. Rams, Exact results for fidelity susceptibility of the quantum Ising model: The interplay between parity, system size, and magnetic field, J. Phys. A **47**, 025303 (2014).

[33] F. Franchini, *An Introduction to Integrable Techniques for One-Dimensional Quantum Systems*, Lecture Notes in Physics (LNP), Vol. 940 (Springer, Cham, 2017).

[34] A. De Pasquale, G. Costantini, P. Facchi, G. Florio, S. Pascazio, and K. Yuasa, XX model on the circle, Eur. Phys. J.: Spec. Top. **160**, 127 (2008).

[35] E. N. Economou, *Green's Functions in Quantum Physics*, 3rd ed., Springer Series in Solid-State Sciences (Springer, Berlin, 2006).

[36] P. W. Anderson, Absence of diffusion in certain random lattices, Phys. Rev. **109**, 1492 (1958).

[37] T. J. G. Apollaro, A. Cuccoli, A. Fubini, F. Plastina, and P. Verrucchi, Entanglement modulation in a spin chain by a local impurity, Int. J. Quantum Inf. **06**, 567 (2008).

[38] V. Coffman, J. Kundu, and W. K. Wootters, Distributed entanglement, Phys. Rev. A **61**, 052306 (2000).

[39] R. Horodecki, P. Horodecki, M. Horodecki, and K. Horodecki, Quantum entanglement, Rev. Mod. Phys. **81**, 865 (2009).

[40] A. Acín, D. Bruß, M. Lewenstein, and A. Sanpera, Classification of mixed three-qubit states, Phys. Rev. Lett. **87**, 040401 (2001).

[41] Y. Hong, T. Gao, and F. Yan, Measure of multipartite entanglement with computable lower bounds, Phys. Rev. A **86**, 062323 (2012).

[42] J. Nocedal and S. J. Wright, *Numerical Optimization*, 2nd ed. (Springer, New York, 2006).

[43] P. Virtanen, R. Gommers, T. E. Oliphant, M. Haberland, T. Reddy, D. Cournapeau, E. Burovski, P. Peterson, W. Weckesser, J. Bright, S. J. van der Walt, M. Brett, J. Wilson, K. J. Millman, N. Mayorov, A. R. J. Nelson, E. Jones, R. Kern, E. Larson, C. J. Carey *et al.*, SciPy 1.0: Fundamental algorithms for scientific computing in Python, Nat. Methods **17**, 261 (2020).

[44] M. Hofmann, A. Osterloh, and O. Gühne, Scaling of genuine multiparticle entanglement close to a quantum phase transition, Phys. Rev. B **89**, 134101 (2014).

[45] L. Gurvits and H. Barnum, Largest separable balls around the maximally mixed bipartite quantum state, Phys. Rev. A **66**, 062311 (2002).

[46] W. K. Wootters, Entanglement of formation of an arbitrary state of two qubits, Phys. Rev. Lett. **80**, 2245 (1998).

[47] L. Amico, A. Osterloh, F. Plastina, R. Fazio, and G. M. Palma, Dynamics of entanglement in one-dimensional spin systems, Phys. Rev. A **69**, 022304 (2004).

[48] R. Lohmayer, A. Osterloh, J. Siewert, and A. Uhlmann, Entangled three-qubit states without concurrence and three-tangle, Phys. Rev. Lett. **97**, 260502 (2006).

[49] C. Eltschka, A. Osterloh, J. Siewert, and A. Uhlmann, Three-tangle for mixtures of generalized GHZ and generalized W states, New J. Phys. **10**, 043014 (2008).

[50] A. Osterloh, J. Siewert, and A. Uhlmann, Tangles of superpositions and the convex-roof extension, Phys. Rev. A **77**, 032310 (2008).

[51] A. F. Abouraddy, B. E. A. Saleh, A. V. Sergienko, and M. C. Teich, Degree of entanglement for two qubits, Phys. Rev. A **64**, 050101(R) (2001).

[52] P. Pandya, O. Sakarya, and M. Wieśniak, Hilbert-Schmidt distance and entanglement witnessing, Phys. Rev. A **102**, 012409 (2020).

[53] S. M. Hashemi Rafsanjani, M. Huber, C. J. Broadbent, and J. H. Eberly, Genuinely multipartite concurrence of N-qubit X matrices, Phys. Rev. A **86**, 062303 (2012).

[54] S. M. Giampaolo and B. C. Hiesmayr, Genuine multipartite entanglement in the cluster-Ising model, New J. Phys. **16**, 093033 (2014).

[55] S. M. Giampaolo and B. C. Hiesmayr, Topological and nematic ordered phases in many-body cluster-Ising models, Phys. Rev. A **92**, 012306 (2015).

[56] M. Consiglio and G. Torre, Defects, 2024, https://github.com/mirkoconsiglio/defects.